The solar influence on the probability of relatively cold UK winters in the future

2011 Environ. Res. Lett. 6 034004

(http://iopscience.iop.org/1748-9326/6/3/034004)

Environ. Res. Lett. **6** (2011) 034004 (11pp) doi:10.1088/1748-9326/6/3/034004

The solar influence on the probability of relatively cold UK winters in the future

M Lockwood[1,2], R G Harrison[1], M J Owens[1], L Barnard[1], T Woollings[1] and F Steinhilber[3]

[1] Space and Atmospheric Electricity Group, Department of Meteorology, University of Reading, Earley Gate, PO Box 243, Reading RG6 6BB, UK
[2] Space Science and Technology Department, Rutherford Appleton Laboratory, Harwell Campus, Chilton, Didcot, Oxfordshire OX11 0QX, UK
[3] EAWAG, Swiss Federal Institute of Aquatic Science and Technology, PO Box 611, Ueberlandstrasse 133, 8600 Dübendorf, Switzerland

E-mail: m.lockwood@reading.ac.uk

Received 8 January 2011
Accepted for publication 8 June 2011
Published 5 July 2011
Online at stacks.iop.org/ERL/6/034004

Abstract
Recent research has suggested that relatively cold UK winters are more common when solar activity is low (Lockwood *et al* 2010 *Environ. Res. Lett.* **5** 024001). Solar activity during the current sunspot minimum has fallen to levels unknown since the start of the 20th century (Lockwood 2010 *Proc. R. Soc.* A **466** 303–29) and records of past solar variations inferred from cosmogenic isotopes (Abreu *et al* 2008 *Geophys. Res. Lett.* **35** L20109) and geomagnetic activity data (Lockwood *et al* 2009 *Astrophys. J.* **700** 937–44) suggest that the current grand solar maximum is coming to an end and hence that solar activity can be expected to continue to decline. Combining cosmogenic isotope data with the long record of temperatures measured in central England, we estimate how solar change could influence the probability in the future of further UK winters that are cold, relative to the hemispheric mean temperature, if all other factors remain constant. Global warming is taken into account only through the detrending using mean hemispheric temperatures. We show that some predictive skill may be obtained by including the solar effect.

Keywords: regional climate, solar variability, blocking

1. Introduction

The central England temperature (CET) data series [5, 6] is the world's longest instrumental temperature record and extends back to 1659, around the beginning of the Maunder minimum in solar activity. The CET covers a spatial scale of order 300 km which makes it a 'small regional' climate indicator but, to some extent, it will also reflect changes on both regional European and hemispheric scales [7]. The mean CET for December, January and February (DJF), T_{DJF}, for the recent relatively cold winters of 2008/9 and 2009/10 were 3.50 °C and 2.53 °C, respectively, whereas the mean value (±one standard deviation) for the previous 20 winters had been (5.04 ± 0.98) °C. The CET for December 2010 was −0.6 °C which makes it the second coldest December in the entire record, the only colder one being in 1889/90; however warmer temperatures in the UK during January and February gave a DJF mean for 2010/11 of 3.13 °C. The cluster of lower winter temperatures in the UK during the last 3 years has raised questions about the probability of more similar, or even colder, winters occurring in the future. For example, because of the resource implications for national infrastructure planning, the probability of further severe winters is of central importance to the 'winter resilience review' announced in the UK Parliament by the Secretary of State for Transport in December 2010 [8].

Many factors influence winter temperatures in the UK. For example, they are closely linked to the phase of the North Atlantic Oscillation (NAO), and associated changes in thermal advection, which contribute a large fraction of the

observed variability of the winter CET values [7]. Hence, the observed increasing trend in the NAO index between 1965 and 1995 has contributed considerably to the warming trend seen in European regional temperatures (including CET) during winter over this interval. Here we restrict our discussion to the evidence for solar modulation of winter CET values (potentially via the NAO) but it should be noted that such modulation is only one of several factors. For example although, as reported by Lockwood *et al* [1], cold winters in the CET record are more likely when solar activity was low, the scatter in the data is extremely large. This is well demonstrated by comparing the winters of 1683/4 and 1685/6: the former is the coldest ($T_{\rm DJF} = -1.2\,^{\circ}$C) and the latter the sixth warmest ($T_{\rm DJF} = +6.3\,^{\circ}$C) of all the winters in the CET record and yet the two were only 2 years apart and both were during the extremely quiet solar conditions of the Maunder minimum. On the other hand, 6 out of the 11 coldest winters ($T_{\rm DJF} < 1.0\,^{\circ}$C) occurred before 1720, during the Maunder minimum, despite it giving just 60 of the 350 observations. Some of this could be due to the effect of global warming on CET values; however after removal of the trend in northern hemispheric temperatures, $T_{\rm NH}$ (yielding $\delta T_{\rm DJF} = T_{\rm DJF} - sT_{\rm NH}$, where s is the slope of the best fit linear regression between $T_{\rm DJF}$ and $T_{\rm NH}$), 6 of the 17 coldest winters ($\delta T_{\rm DJF} < 1.4\,^{\circ}$C) are still found within the Maunder minimum [1]. From the above, it is clear that, on its own, solar activity is very a poor predictor of the winter temperature in the UK in any one year. Indeed, other studies have found the recent winters to be consistent with internal variability alone [71]. In this paper we investigate if using solar activity may have some application in evaluating the likelihood of the occurrence of cold winters on decadal timescales, which requires that an increase in forecast skill be demonstrated.

Modelling studies (e.g., [9–11]) have found that even though solar-induced changes in the global mean air surface temperature are very small, regional and seasonal temperature changes associated with solar variability can be more substantial. In the northern hemisphere, these seem to occur primarily through a forced shift towards the low index state of the Arctic oscillation (AO) and NAO with slight decreases in solar irradiance. This shift is associated with lower temperatures (by 1–2 °C) over the Northern Hemisphere continents, especially in winter, in agreement with historical records and proxy data for surface temperatures. Using a stratosphere-resolving global circulation model (GCM), it has also been reported that long-term regional changes during the pre-industrial period could have been dominated by solar forcing [11] and studies of palaeoclimate data give some support to solar effects influencing the so-called 'little ice age' associated with the Maunder minimum and the earlier 'mediaeval maximum', at least in Eurasia.

Using temperature measurements made after the industrial revolution, North and Stevens [12] applied optimal signal detection theory to data from 36 regions around the globe and found the solar signals were small and not highly significant. On the other hand, multivariate fits by Lean and Rind [13] reveal strong solar responses in certain regions, and Eurasia in particular. Statistical analyses detecting small signals require appropriate and robust statistical methods. As a result, although signatures of multidecadal solar variability in European atmospheric temperatures have recently been reported as statistically significant by Kossobokov *et al* [14] and Le Mouël *et al* [15–17], debate continues. For example, Yiou *et al* [18] and Legras *et al* [19] argue that these findings are insufficient to reject the null-hypothesis that the signatures only result from internal variability. Recent detection–attribution studies, however, do reveal external forcing of pre-industrial winter European temperatures, although signals are weaker than for global mean temperatures [20]. It should be noted that regional/seasonal signatures that have been proposed as solar in origin have also been attributed to the influence of El-Niño/La-Niña on the state of the NAO [21], as a consequence of land use or as originating from internal variability [22, 71]. The CET observations form a very valuable dataset because the data sequence is homogeneous, yet of sufficient length to allow relatively weak signals to be detected with statistical significance. They are also important because they cover an interval containing both a grand solar minimum (the Maunder minimum) and a grand solar maximum (recent decades) and so encompass almost the full range of known solar activity variations.

Several mechanisms have been proposed whereby solar variability could influence European winter temperatures. Early instrumental records from the Maunder minimum indicate an increased frequency of easterly winds influencing the UK temperatures in winter. This has also been deduced from indirect proxies [23], including the spatial patterns of changes in recorded harvest dates [24]. Such a prevalence of wind direction suggests a link with long-lived 'blocking events' in the eastern Atlantic at low solar activity. Blocking episodes comprise extensive and quasi-stationary anticyclones that can persist for several weeks, leading to extended cold periods in winter as the mild maritime westerly winds are replaced by continental north-easterlies. Depending on the position of the anticyclone, cloud free skies may also be produced, permitting appreciable nocturnal cooling of land with limited daytime warming during short winter days. Long-lived Atlantic blocking events at more eastward locations have been associated with colder winters in Europe and have been found to be significantly more prevalent at sunspot minimum than at higher solar activity [25, 26].

Other evidence supports a solar influence amplified to modify circulation patterns. For example, the effects of the changed position and frequency of blocking events may be viewed as a manifestation of modes of low-frequency circulation variability that have been found to respond to solar activity, giving increased/decreased frequencies of easterly/westerly circulation patterns over Europe under low solar activity conditions [27, 28]. Winter CET values are known to be strongly modulated by the NAO [7] and modelling has shown that stratospheric trends over recent decades, along with downward links to the surface, are indeed strong enough to explain much of the prominent trend in the NAO and hence regional winter climate in Europe between the 1960s and the 1990s [29]. This is supported by known connections between the state of the stratosphere

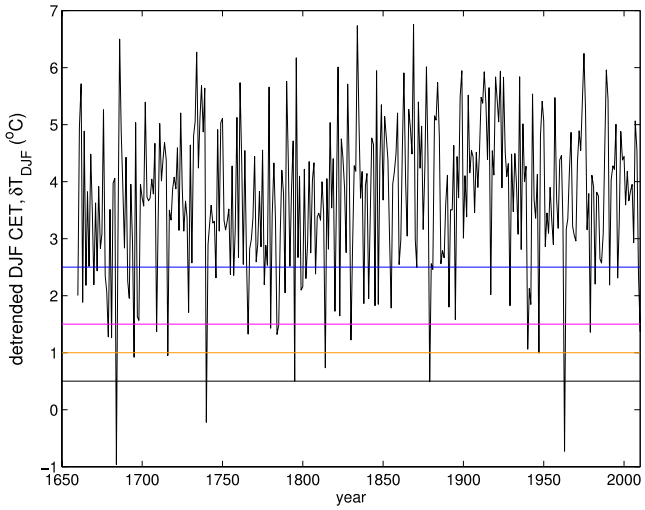

Figure 1. The variation of $\delta T_{\rm DJF}$, the December/January/February (DJF) means of central England temperatures, detrended using northern hemisphere means and the procedure described by Lockwood *et al* [1]. The thresholds shown are at 2.5 °C (blue), 1.5 °C (mauve), 1.0 °C (orange), and 0.5 °C (black). The numbers of the 336 annual values (with simultaneous solar data) below these thresholds are 60, 20, 9 and 4, respectively, giving overall occurrence frequencies of 17.9%, 6.0%, 2.8% and 1.2%.

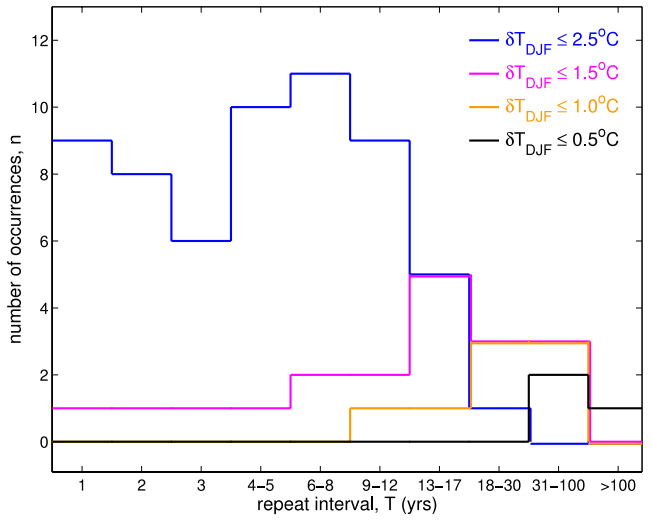

Figure 2. The distributions of intervals T between winters with $\delta T_{\rm DJF}$ below the four thresholds shown in figure 1. The colour scheme used for the four thresholds is as in figure 1. Note that the width of bins in the histograms increases nonlinearly to the right.

and the occurrence of blocking events [30, 31] and by GCM simulations which produce a relative negative phase of the NAO/AO during the Maunder minimum which contributes to the lower European winter temperatures [32]. A viable mechanism associates variations in solar UV emissions [33] with changes to stratospheric temperatures and winds [34]. These could influence the underlying troposphere through disturbances to the stratospheric polar vortex [35] which may propagate downwards to affect the tropospheric jets, or through the effects of stratospheric temperature changes modifying the refraction of tropospheric storm-track eddies [36].

2. Winter central England temperatures

Figure 1 shows the detrended winter CET dataset developed by Lockwood *et al* [1]. The effect of hemispheric change on the raw CET data has been removed by cross-correlation with the HadCRUT3 data composite of northern hemisphere observations, extended back to the start of the CET dataset using the median of a basket of palaeoclimate reconstructions. This influence is then subtracted to give the detrended values, $\delta T_{\rm DJF}$, shown. Note that by using $\delta T_{\rm DJF}$ rather than the absolute temperatures, we here study the deviation of UK temperatures from hemispheric means and hence the variation of winter UK temperatures around the trend expected for the northern hemisphere due to global warming. We therefore describe low-$\delta T_{\rm DJF}$ winters as 'relatively cold'. There are 350 annual $\delta T_{\rm DJF}$ values, 336 of which have simultaneous open solar flux estimates. Also shown in figure 1 are three threshold values of $\delta T_{\rm DJF}$ that are used in the present paper to define relatively cold winters: 2.5, 1.5, 1.0, and 0.5 °C (shown, respectively, by the blue, mauve, orange and black horizontal lines). The numbers of the 336 annual $\delta T_{\rm DJF}$ values below these thresholds are 60, 20, 9 and 4, respectively, giving overall occurrence frequencies of 18, 6, 3 and 1.2%. To put these thresholds into context: the lowest $\delta T_{\rm DJF}$ value in the 351-year record is that for 1683/4 which is $\delta T_{\rm DJF} = -0.96$ °C, the second lowest is $\delta T_{\rm DJF} = -0.73$ °C in 1962/3 and last year (2009/10) was the 18th lowest with $\delta T_{\rm DJF} = +1.37$ °C.

Figure 2 shows the intervals T between relatively cold winters, defined by when $\delta T_{\rm DJF}$ falls below the thresholds shown in figure 1. In this plot, and in all subsequent ones, we employ the same colour scheme for the four thresholds shown in figure 1. Notice that the bin widths are not constant in this figure. For $\delta T_{\rm DJF} \leqslant 2.5$ °C there is a tendency for colder winters to cluster with many following shortly after the previous one: for example in 44 out of 59 cases T is less than 5 years for this threshold. However for $\delta T_{\rm DJF} \leqslant 1.5$ °C this is less true as a smaller fraction (only 4 out of 19 cases) give T less than 5 years; for $\delta T_{\rm DJF}$ below 1.0 and 0.5 °C there are no T values less than 9 years and 30 years, respectively. Hence the tendency to cluster is a feature of moderately cold winters but not of the coldest winters, relative to the hemispheric mean temperature. The $\delta T_{\rm DJF}$ values for 2008/9, 2009/10 and 2010/11 are 2.37, 1.37 and 1.94 °C, respectively: figure 2 shows that two successive winters below 2.5 °C is somewhat but not excessively unusual (it has happened nine times in the past 350 years). That $\delta T_{\rm DJF}$ fell below the 2.5 °C threshold for the last three years in a row is more unusual, it having happened only twice previously. Had $\delta T_{\rm DJF}$ fallen below 1.5 °C in 2010/11, as it did in the previous year, this would have been very unusual indeed (it has happened just once in the entire 350-year series).

As in the previous study by Lockwood *et al* [1], we use the open solar flux $F_{\rm S}$—the total magnetic flux dragged out of the Sun's atmosphere by the solar wind flow. This can be estimated from terrestrial observations of geomagnetic activity [37, 38]. Comparison with satellite observations shows the method is extremely reliable, even during the current exceptional solar

minimum [2]. Open solar flux is highly anticorrelated with the fluxes of galactic cosmic rays (GCRs), and hence with the abundances of cosmogenic isotopes produced by GCRs; it also correlates very well (with a lag of 1 year) with total solar irradiance (TSI) [1]. There are intercalibration and calibration drift uncertainties in composites of data on UV spectral irradiance, but there are indications that open solar flux might be a valuable proxy for solar UV emissions at the wavelengths responsible for ozone production and stratospheric heating [33, 72]. Woollings *et al* [26] have shown that the occurrence of long-lived winter blocking events influencing Eurasian temperatures is strongly related to F_S over recent decades. The sequence of F_S data from geomagnetic data has been extended back to the Maunder minimum using the model of Vieira and Solanki [39] based on the observed sunspot number R, and in very good agreement with both cosmogenic isotope abundance data and reconstructions of TSI [40, 41, 38]. The key finding of the previous study [1] is reproduced here in figure 3(a), a scatter plot of δT_{DJF} against F_S. The figure also shows the four threshold δT_{DJF} values. For δT_{DJF} below all four thresholds, almost all cases occur at lower F_S and the relative absence of points in the bottom-right quadrant of figure 3(a) (low δT_{DJF}—high F_S cases) was shown in [1] to be statistically significant at the 99% level.

We here aim to derive an algorithm to predict the probabilities of δT_{DJF} below the four thresholds as a function of the open solar flux (F_S) and to test if this algorithm gives any improvement in predictive skill. To do this, we divide the data into two halves, the first is used to generate the algorithm, the second used for an independent test of the algorithm. Because the long-term trend in the data is an important factor it is important that both fitted and test subsets of the data sample both the high and low F_S conditions of the Maunder minimum and the recent grand solar maximum, respectively. We here use all odd-numbered years to derive the algorithm (the 'fit data set') and all the even-numbered years to test it (the 'test data set'). Reversing these roles made no difference to the conclusions reached.

Using the fit data set, the fraction of winters with δT_{DJF} below a given threshold was evaluated for subsets with F_S below a threshold value which was varied between 0.25×10^{14} Wb and 6×10^{14} Wb in steps of 0.25×10^{14} Wb. These cumulative probabilities $C_{<F_s}$ are shown by the points in figure 3(b) for the same four δT_{DJF} thresholds as used in the previous figures. To turn these cumulative probability distributions into differential ones (and hence obtain the probability densities) they must be differentiated and fluctuations due to small sample numbers will cause large variations. Thus it is necessary to fit the distributions with a smooth polynomial. It is also desirable to use the same polynomial form for the different thresholds as this avoids the potential for the fits to generate higher probabilities for lower δT_{DJF} thresholds and has the advantage of increasing the number of available data points. This was achieved by scaling all the distributions so that they varied between zero (at the largest observed F_S of 6×10^{14} Wb) and unity (at $F_S = 0$) and then fitting a fifth-order polynomial to the normalized data for all four thresholds, constrained to pass through the two endpoints. The polynomial order used was the highest possible without oscillatory behaviour in the fit setting in: a behaviour that was not consistent when the data for the four thresholds were fitted separately. Using a fourth, or even a third-order polynomial did not substantially alter the fits obtained. This functional form was then scaled to give the best least-squares fit

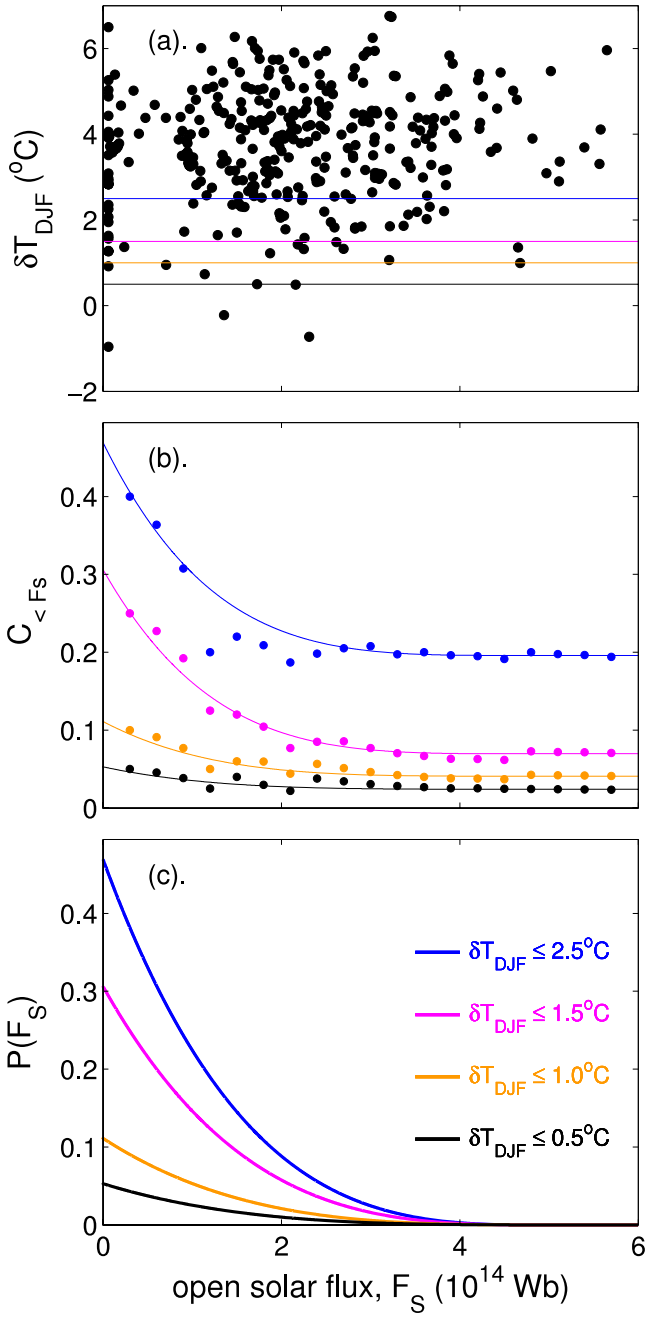

Figure 3. (a) Scatter plot of detrended winter CET values δT_{DJF} as a function of the open solar flux F_S, as derived and presented in [1]. Also shown are the threshold δT_{DJF} values shown in figure 1. (b) The cumulative probabilities $C_{<F_s}$ of δT_{DJF} being at or below the four thresholds for open solar flux F_S at or below the threshold value given by the ordinate of the plot. The points are observed values for odd-numbered years for 0.25×10^{14} Wb steps in the F_S threshold; the lines are best fit fifth-order polynomial (see discussion in text). (c) Probability densities, $P(F_S)$, derived by differentiation of the fitted $C_{<F_s}$ curves in part (c).

Table 1. Median values of predicted probabilities, $P(F_S)$ for above and below the four δT_{DJF} thresholds and the confidence level of the difference between the two evaluated using the Wilcoxon (Mann–Whitney) U test. (a) is for all years in the test data set, (b) excludes data from the test data set within 4 years of a tropical volcanic eruption (see text for details).

δT_{DJF} threshold (°C)	2.5	1.5	1.0	0.5
(a) All test data				
Median $P(F_S)$ for δT_{DJF} below threshold	0.112	0.073	0.051	0.033
Median $P(F_S)$ for δT_{DJF} above threshold	0.070	0.046	0.016	0.008
Significance of difference in medians (%)	90.32	83.10	98.12	91.10
(b) Test data excluding years following tropical volcanoes				
Median $P(F_S)$ for δT_{DJF} below threshold	0.112	0.073	0.051	0.033
Median $P(F_S)$ for δT_{DJF} above threshold	0.059	0.038	0.014	0.007
Significance of difference in medians (%)	94.10	90.82	98.51	92.10

to each of the four sets of data points in figure 3(b) individually, giving the solid curves shown. It can be seen that the fits are not perfect, but they are reasonable given the low numbers of data samples available. Because the fitted curves are a smooth polynomial, they could be differentiated to give the probability densities $P(F_S)$ as a function of F_S that are shown in figure 3(c). Each curve has been normalized so that the integral over the full range of observed F_S (between 0 and 6×10^{14} Wb) yields the observed total probability for that threshold δT_{DJF} value.

To test this algorithm, we used the independent test dataset. Figure 4 shows the predicted probability of δT_{DJF} being below one of the four thresholds, $P(F_S)$, as a function of the actual δT_{DJF} observed. The vertical lines give the four δT_{DJF} thresholds using the same colour scheme as previous figures. The vertical (probability) axis is normalized to the maximum value at $F_S = 0$, $P(F_S = 0)$, for the δT_{DJF} threshold in question. Because the fitted curves in figures 3(b) and (c) have the same functional form for all the thresholds, this normalized variation is the same for all four thresholds in figure 4. The behaviour in the figure is as would be predicted from the scatter in figure 3(a) which shows that low solar activity does not guarantee a relatively cold winter: as a result, at high δT_{DJF} a full range $P(F_S)$ is predicted but at low δT_{DJF} the $P(F_S)$ values are higher. For the inclusion of the solar factor to give any chance of an improvement in prediction skill, it is necessary that $P(F_S)$ for below the threshold be significantly higher than for above it. Table 1 tests this by taking median values of $P(F_S)$ for years with δT_{DJF} above and below each threshold and evaluating the significance of the difference between them using the Wilcoxon (Mann–Whitney) U test.

Part (a) of table 1 applies this test to all data in the test set. The median $P(F_S)$ is consistently higher for the winters with temperatures below the thresholds, but the confidence level of the difference is not uniformly high for all thresholds (varying between 83 and 98%). The reason higher significances are not obtained is the large number of 'false positives', i.e. years in which $P(F_S)$ is high and yet δT_{DJF} does not fall to low values. As will be discussed below, there a large number of potential reasons for this, but one in particular is relatively well understood and we can make a simple allowance for it. It is known that large tropical volcanoes tend to induce positive NAO and hence give warmer winters in Europe. This

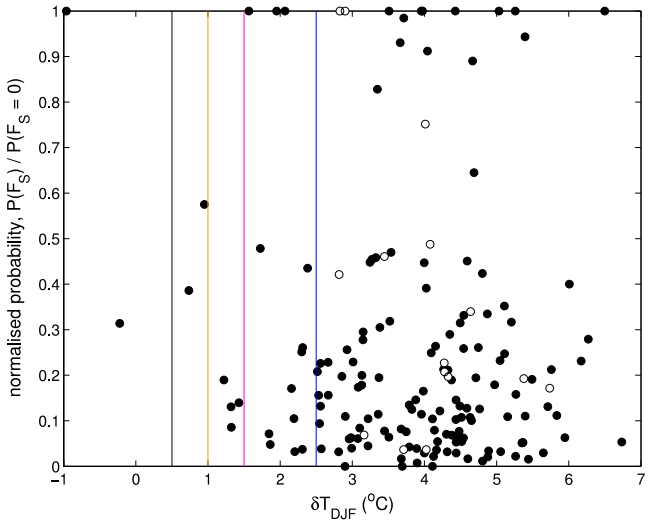

Figure 4. Analysis of the test data provided by even-numbered years. The predicted probability of δT_{DJF} below one of the four thresholds from the annual F_S value, $P(F_S)$, normalized to the peak value (for $F_S = 0$) for that threshold, $P(F_S = 0)$, is shown as a function of the observed δT_{DJF} value. Because the same functional form is used for all four thresholds, the normalized probability has the same form in all four cases. The vertical coloured lines give the thresholds. Open circles denote winters that are within 4 years of a major tropical volcano (defined as giving mean atmospheric optical depth >0.05 in mean the ice-core volcanic index 2 (IVI2) at latitudes between 30°N and 30°S).

'winter warming effect' [42, 43] contrasts the summer cooling effect of volcanoes and has been simulated in GCM climate models [44] and detected in reconstructions of European temperatures [20, 45]. We here use the ice-core volcanic index 2 (IVI2) [46] to define years when the atmospheric optical depth due to sulfate loading exceeds 0.05, averaged over the latitude band 30°S–30°N. The winter warming effect is typically seen 2–3 winters after an eruption [20, 44]. In figure 4, the open circles are for winters within 4 years of a defined tropical volcano. It can be seen that for such years there are no lower δT_{DJF} values. In part (b) of table 1, these years are excluded from the test on the grounds they may have been subject to volcanic winter warming: the differences between the medians are increased slightly, so that the significance values are then all elevated to above 90%.

3. Predicting the future variation of open solar flux

The distributions given in figure 3(c) allow us to compute a probability of a given detrended winter temperature for a given value of the open solar flux, F_S. Thus to predict the solar influence on future probabilities of cold UK winters (relative to the hemispheric mean), we also need to predict how open solar flux will evolve. At the present time, models of the solar dynamo do not give a forecasting capability [47]; therefore we have to use past experience to evaluate statistically how the open solar flux is likely to evolve in the future. Fortunately, we have a long data record of solar activity because the open magnetic field of the Sun shields Earth from GCRs, which generate spallation products (such as the two cosmogenic radionuclides ^{10}Be and ^{14}C) on hitting the atmosphere. These cosmogenic isotopes precipitate and are stored in terrestrial reservoirs such as tree trunks and ice sheets. Samples taken from cores into these reservoirs can be dated and the variation of the abundances of the cosmogenic isotopes, after removal of complicating factors such as the variability of the shielding afforded by the geomagnetic field, reveal the effect of the Sun in modulating the fluxes of GCRs reaching the Earth [48]. As a result, cosmogenic isotopes provide unique insight into solar variability on a wide range of timescales from years to millennia. Such analyses all indicate that the Sun has been unusually active over recent decades [49–53]; however, there are differences between the various reconstructions. For example, Solanki *et al* [49] used the ^{14}C cosmogenic isotope abundance found in tree trunks and concluded that the Sun has been more active in recent decades than at any time in the previous 8000 years and that it was as active as in recent decades for only 10% of the past 11 000 years. Vonmoos *et al* [50] employed ^{10}Be from the Greenland ice-core project (GRIP) ice core in addition to ^{14}C. Their reconstruction is similar to that by Solanki *et al* but not identical; however, it did not include the recent grand maximum as it ended at 390 years before the present day. Muscheler *et al* [51] also used both ^{10}Be and ^{14}C and their reconstruction is more significantly different to that of Solanki *et al* in that, although recent activity was found to be high, it was not quite as exceptional, being at levels that were found for 20% of the time. A comparison of modern and historic data was recently achieved by Steinhilber *et al* [53] by using numerical modelling to combine ^{10}Be data with modern neutron monitor data. As in the former studies [49–52], Steinhilber *et al* obtained the solar modulation potential ϕ from the radionuclide data by deducting the shielding effect of the geomagnetic field and using Monte Carlo calculations of cosmogenic isotope production (e.g., [54]): ϕ quantifies the GCR shielding effect of the heliosphere [55] and is a good parameter for describing solar modulation of GCRs at Earth. The dataset of Steinhilber *et al* comprises 25-year means of ϕ and covers the past 9300 years.

The results of Steinhilber *et al* [53] show considerable agreement with the heliospheric field strength and open solar flux variations derived since the Maunder minimum from geomagnetic activity observations [56, 38]. Figure 5 shows the variation of the 25-year means of F_S, $\langle F_S \rangle_{25}$, derived from

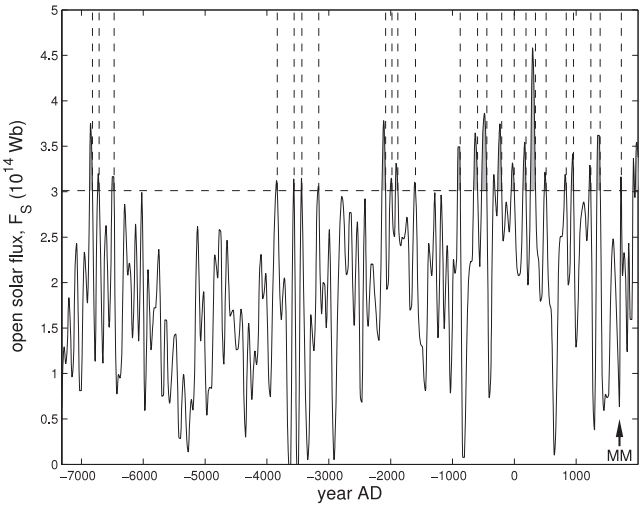

Figure 5. The variation of open solar flux F_S (25-year means) over the last nine millennia derived from the heliospheric GCR modulation parameter ϕ composite compiled from Steinhilber *et al* [52], here converted into F_S using the best fit linear regression $F_S = 5.06 \times 10^{11}$ (ϕ in MV) Wb [37]. The grey-shaded areas are grand solar maxima, defined as when ϕ exceeds the 600 MV level (corresponding to the $F_S = 3.04 \times 10^{14}$ Wb level shown by the horizontal dashed line). The vertical dashed lines mark the ends of the 24 grand solar maxima (at times t_0) before the current one. The arrow labelled MM marks the Maunder minimum.

the ϕ variation of Steinhilber *et al* using the simple linear regression $\langle F_S \rangle_{25} = 5.06 \times 10^{11}$ (ϕ in MV) Wb [38]. (Note that $F_S = 0$ when $\phi = 0$.) It can be seen that recent decades have been within one of the 25 maxima (called 'grand solar maxima') in this interval. The vertical dashed lines mark the ends of the 24 grand solar maxima preceding the current one (at times t_0), defined as when ϕ falls below the 600 MV level. This corresponds to the $\langle F_S \rangle_{25} = 3.04 \times 10^{14}$ Wb level shown by the horizontal dashed line in the figure which, using the linear extrapolation in figure 11 of paper [4], is very close to the estimated value for $\langle F_S \rangle_{25}$ for 2010.

Using the same ϕ reconstruction, Abreu *et al* [3] showed that the current grand solar maximum was unusually long-lived and so inferred that it is due to end soon. Lockwood and Fröhlich [57] noted that solar activity levels have been declining since 1985 and the recent relatively low minimum of the 11-year solar cycle is consistent with this decline [2]. By extrapolation of the F_S variation derived from geomagnetic activity data, Lockwood *et al* [4] estimate that the current grand solar maximum will end by 2014, consistent with the range of possibilities derived from the distribution of duration of grand solar maxima by Abreu *et al* [3]. Subsequent data in the recent low solar minimum refine this best estimate to 2013 with an uncertainty of ±2 yr. Lockwood [2] used a superposed epoch (compositing) technique, by adopting the 24 endings of previous grand solar maxima as a timing pulse to study the typical subsequent evolution of ϕ and found that there was a probability of 2/24 (≈8%) that the Sun would return to Maunder minimum conditions within the next 40 years.

Figure 6 shows a composite of the 24 variations over intervals of 200 years around the times t_0 when $\langle F_S \rangle_{25}$ falls

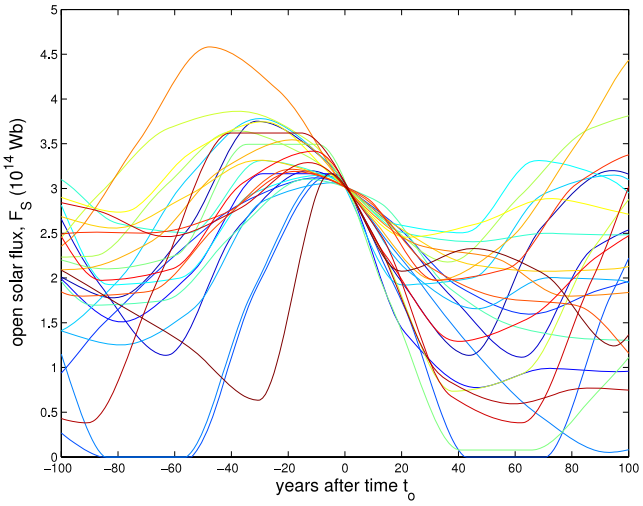

Figure 6. Composite of the 24 variations of the open solar flux F_S shown in figure 5 around the times t_0 (shown in figure 5 by the vertical dashed lines). The variations shown are annual values interpolated from the 25-year values using cubic splines.

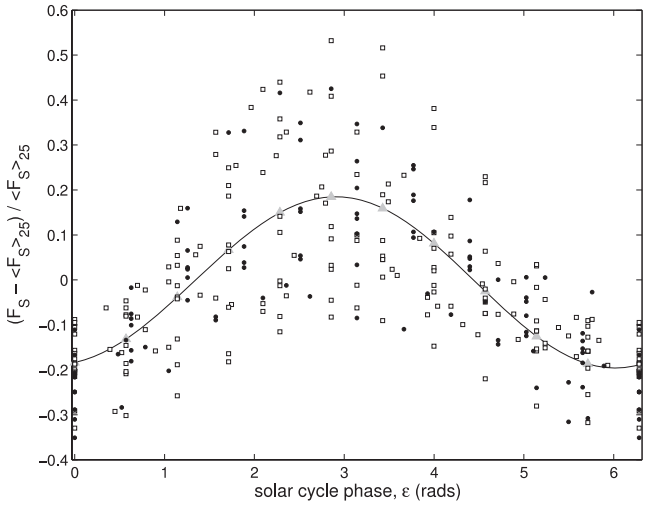

Figure 7. The solar cycle variation in open solar flux F_S. The points are values of the ratio $(F_S - \langle F_S \rangle_{25})/\langle F_S \rangle_{25}$ where F_S and $\langle F_S \rangle_{25}$ are annual and 25-year means of open solar flux: solid circles are from geomagnetic activity data for 1900 and after [4], open squares are for the model reconstruction for 1720–1989 [38]. The solar cycle phase ε of each annual value is calculated between the prior and subsequent minima in F_S. The solid line is an eighth-order polynomial fit (with periodic boundary conditions) to the F_S values for all years (1720–2010) and the grey triangles are annual values for an 11-year solar cycle.

below the 3.04×10^{14} Wb level (the vertical dashed lines in figure 5). Most examples show a decline to a minimum within the 100 years after t_0 but the depth and timing of that minimum varies considerably. These data have been converted from the 25-year means into annual values using cubic spline interpolation. Hence they do not allow for the decadal scale solar cycle variation in F_S. To study the solar cycle variation around the 25-year means, figure 7 shows the average variation over the solar cycle of F_S normalized to the 25-year running mean value for the same year. This plot uses the annual F_S data derived from geomagnetic activity for 1900 onwards [4] (solid circles) and the model extension to earlier years [39] (open squares). For each year (date t), the phase of the solar cycle is calculated as $\varepsilon = 2\pi(t - t_1)/(t_2 - t_1)$, where t_2 and t_1 are the dates of the subsequent and prior minimum in F_S, respectively. The figure covers 1720–2010 for which t_2 and t_1 can be readily identified. The plot shows the variation of the deviation from the 25-year means, $(F_S - \langle F_S \rangle_{25})$ as ratio $\langle F_S \rangle_{25}$ and as a function of ε. The scatter is considerable, some of which is caused by the effect on ε of the variation of solar cycle length $(t_2 - t_1)$ when using annual data; the rest is due to cycle-to-cycle variability. An eighth-order polynomial fit to all the cycles, with periodic boundary conditions, is also shown and the grey triangles show annual values for the average solar cycle length $(t_2 - t_1)$ of 11 years. This fit provides an approximate method of adding a solar cycle variation to the 25-year means because F_S can be computed from $\langle F_S \rangle_{25}$. Two examples are given in the top panels of figure 8. The left-hand example is for a grand solar maximum that ended at t_0 of 1980 BC and the right-hand example is for the example at t_0 of 875 BC. In each case the green line is the variation shown in figure 6 and the black line has been modulated by the best fit solar cycle phase variation shown in figure 7. There is a weak relationship between solar cycle length $(t_2 - t_1)$ and $\langle F_S \rangle_{25}$ but its use here would not be justified, considering the variability of the data around the best fit polynomial in figure 7. Hence we assume a constant solar cycle length of 11 years. In addition, we assume that time t_0 is at a solar minimum, as is approximately the case at the present time. Of the 24 examples shown in figure 6, the example for $t_0 = 1980$ BC (left) shows the least deep minimum after the time t_0. We assume that all variations are equally probable following the end of the current grand solar maximum and so there is a probability of 1/24 (4.2%) that the future evolution of F_S will be similar to that shown in this plot. The plot for $t_0 = 875$ BC, on the other hand, represents the opposite extreme with a rapid descent to grand solar minimum. Figure 6 shows that this (i.e. $F_S \approx 0$) occurs in two out of 24 cases and so the probability is 2/24 (=8.4%).

4. Predicting the future probabilities of relatively cold UK winters

The bottom panels of figure 8 show the probability P_T of δT_{DJF} being below the four thresholds shown in figure 1, using the variations of F_S shown in the upper panels with the probability densities presented in figure 3(c). For the $t_0 = 1980$ BC event (left), the probabilities are only weakly and briefly enhanced and the main feature is the weak solar cycle oscillation. On the other hand, for the $t_0 = 875$ BC event (right), probabilities rise to about 32%, 15%, 8% and 3% for detrended mean winter CET temperatures δT_{DJF} below the thresholds of 2.5 °C, 1.5 °C, 1.0 °C, and 0.5 °C, respectively. These probabilities are roughly twice those for the whole dataset (i.e. 1659–2010), which are 18%, 6%, 3% and 1.2%. These probabilities also match (and, for the coldest winters, slightly exceed) those observed during the Maunder minimum (consistent with the fact that the predicted F_S falls to values slightly lower than

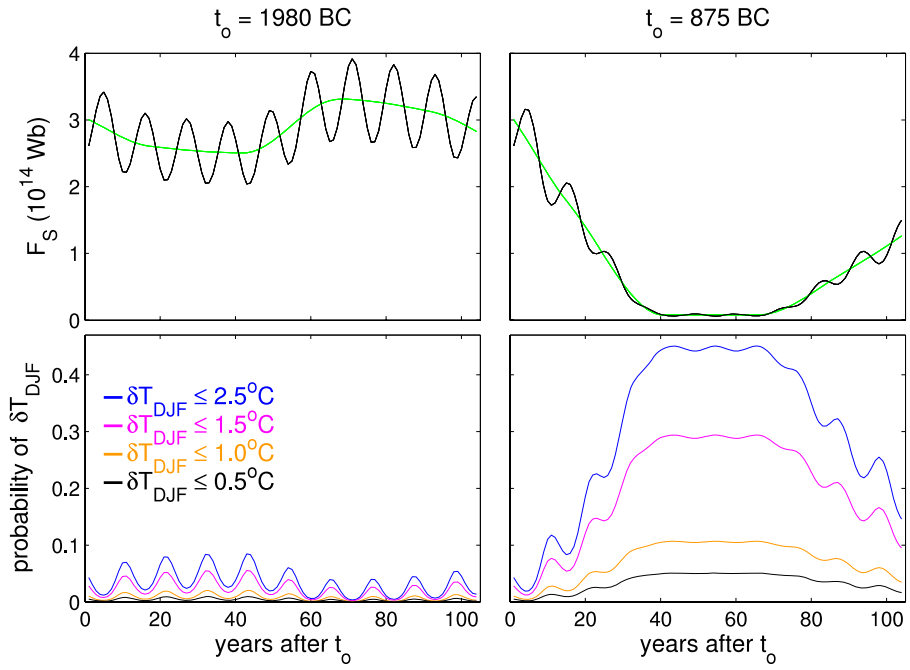

Figure 8. Two examples of variations after the end of a grand solar maximum: (left) for $t_0 = 1980$ BC and (right) for $t_0 = 875$ BC. The top panels show the open solar flux variation: the green line is as presented in figure 6 and this has been modulated by the solar cycle phase variation shown in figure 7 (assuming a constant solar cycle length of 11 years) to give the black line. The bottom panels show the probability that $\delta T_{\rm DJF}$ is below the four thresholds shown in figure 1, using the probability densities shown in figure 3(c) and the same colour scheme as previous plots.

those derived for the Maunder minimum): for 1659–1700 the percentages of winters with $\delta T_{\rm DJF}$ below the four thresholds are 37.5%, 10.0%, 5.0% and 2.5%.

To compute the overall probability we calculate $\Sigma_j P_j P_T$, where the sum is over all 24 of the exits from the grand solar maxima shown in figure 6. Because we consider each case to be equally probable, we assign $P_j = 1/24$ for all j. The results for the four thresholds are shown in figure 9. The solid lines assume the grand solar maximum ends in 2013 and the shaded areas give the effect of an uncertainty of ± 2 yr around this date.

It can be seen that the probability falls over the next few years as sunspot activity rises with the new solar cycle. However, because of the long-term decline in $\langle F_{\rm S} \rangle_{25}$, the predicted $F_{\rm S}$ for the next solar minimum is lower than during the current minimum and so the probabilities rise to greater values. This is repeated over the subsequent three solar cycles until the solar minima 45–55 years into the future yield peak probabilities near 18%, 12%, 4% and 1.5%, for $\delta T_{\rm DJF}$ below 2.5 °C, 1.5 °C, 1.0 °C, and 0.5 °C, respectively. These values are close to the corresponding averages for the whole interval covered by the CET dataset (1659–2010, which includes one grand solar maximum and one grand solar minimum), which are shown by the horizontal dashed lines in figure 9. However they are larger than the observed occurrence frequencies for the decade before the recent solar minimum (1998–2008, all within the recent grand solar maximum) which are 0 for all four $\delta T_{\rm DJF}$ thresholds.

Note that the solar cycle oscillations are in figure 9 are relatively small. They are largest for the $\delta T_{\rm DJF}$ threshold of 2.5 °C, but sunspot minimum is currently only 3.5% more likely to give a relatively cold winter than sunspot maximum and even at the peak of the long-term variation shown in figure 9, this figure is only 5%. The centennial scale solar

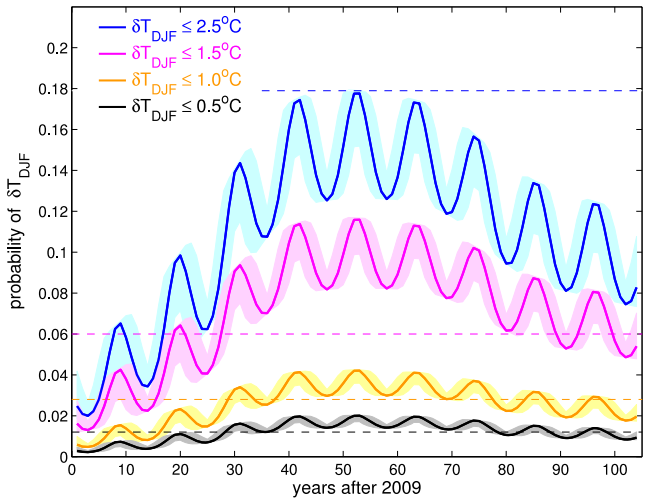

Figure 9. The probability that the detrended winter CET $\delta T_{\rm DJF}$ is below the four thresholds shown in figure 1, based on the 24 exits from a grand solar maximum shown in figure 6. Each of the 24 observed variations after time t_0 are deemed equally likely and so each is assigned a probability of (1/24). The horizontal dashed lines are the occurrence frequencies of winters with $\delta T_{\rm DJF}$ below the four thresholds in the full 350 years of the CET dataset. The lines are based on the assumption that the end of the grand solar maximum is in 2013, the shaded areas give the range of behaviours for an uncertainty of ± 2 years in that date.

variation, on the other hand increases the probability by of order 12%. All these numbers are reduced if a lower $\delta T_{\rm DJF}$ threshold is considered.

5. Discussion and conclusions

First, we have analysed the probability of cold UK winters (relative to the hemispheric mean temperature) as a function of the open solar flux, using the December/January/February means of the observed Central England Temperatures (detrended to allow for the effect of the rise in hemispheric mean temperatures). Secondly, we have analysed the probabilities of future evolution of open solar flux by looking at cosmogenic isotopes data from times which appear to match the present day, using the assumption that the end of the current grand solar maximum is imminent [3, 4].

By combining the results of these two probability analyses, we find that the solar effect on the probability of relatively cold winters is that they are likely to increase in frequency during the next century, if all other factors remained the same. The observed occurrence frequency, for all four thresholds considered, was zero for the decade prior to the recent low solar minimum (1998–2008), but over the next 50 years, the predicted occurrence of cold winters rises back towards the observed average occurrence for the whole 350-year CET dataset.

However, as stressed above, this analysis assumes that all other factors which can modulate UK winter temperatures remain the same, which is unlikely to be a valid assumption. In addition to giving global-scale warming (e.g., [58]), anthropogenic climate change yields regional changes [20] arising from the dynamical response of the climate system [59], such as changes in ocean circulation [60], sea-ice loss [61, 62] or stratospheric circulation [63]. This reflects the wide range of phenomena that can influence the North Atlantic jet stream and its associated effects on UK winter climate, as described by the NAO. The jet stream exhibits pronounced variability on inter-annual to decadal timescales, some of which may be forced by oceanic [64] or stratospheric [65] variability. Transient events such as volcanic eruptions (e.g., [66]), beyond and including the winter warming effect [42–45] and quasi-periodic variations such as ENSO [67, 68] can also have an influence. However, a large fraction of the variability will reflect the chaotic 'climate noise' of internal atmospheric variability [69, 71]. All of the above contribute to the great scatter seen in figure 4; nevertheless some, if limited, forecast skill remains and can be used because of our analogue forecast of solar activity based on cosmogenic isotope data.

We stress that we have studied the winter UK temperatures relative to the hemispheric means, $\delta T_{\rm DJF}$, rather than the absolute temperatures $\delta T_{\rm DJF}$. Thus our results show how the postulated solar effects might contribute to an increase in the number of anomalously cold UK winters in times when global mean temperatures are rising.

We can, however, place the changes in $\delta T_{\rm DJF}$ discussed in this paper into some context using a simple comparison with the likely effects of global warming on winter CET values. Using the (moderate) IPCC emissions scenario A1B (which gives predicted global temperature rises close to the median for all scenarios [60]), climate models predict that by 2050, (when figure 9 predicts that the probabilities of solar-induced relatively cold winters will peak), the global mean air surface temperature (GMAST) will have risen by about $1.3 \pm 0.4\,^{\circ}$C. The regression used to give $\delta T_{\rm DJF}$ by removing the effect on winter CET of the rise in northern hemisphere mean temperature, $T_{\rm NH}$, has a slope of $s = 1.43 \pm 0.10$ (see figure 3(b) of [1]). If we take the change in $T_{\rm NH}$ to be approximately the same as that in GMAST, we get that the rise in mean winter CET, relative to which $\delta T_{\rm DJF}$ is measured ($\delta T_{\rm DJF} = T_{\rm DJF} - s T_{\rm NH}$) should be $(1.43 \pm 0.10) \times (1.3 \pm 0.4) = 1.9 \pm 0.6\,^{\circ}$C. This simple estimate is very close to the $2.2\,^{\circ}$C rise derived by the UKCP09 study [70]. The average $\delta T_{\rm DJF}$ for recent decades (1988/9–2007/8) has been $4.1\,^{\circ}$C and so the four $\delta T_{\rm DJF}$ thresholds used here (2.5, 1.5, 1.0 and $0.5\,^{\circ}$C) are, respectively, 1.6, 2.6, 3.1 and $3.6\,^{\circ}$C lower than the mean for recent decades. Thus, if the factors are simply superposed, i.e. they do not interact, the lower $2.5\,^{\circ}$C threshold discussed here is likely to yield winters of comparable mean temperature to those seen in the past 20 years, whereas the other $\delta T_{\rm DJF}$ thresholds (1.5, 1.0 and $0.5\,^{\circ}$C) would correspond to winters colder than this by about 1, 1.5 and $2.0\,^{\circ}$C, respectively.

Acknowledgment

The authors are grateful to the staff of the UK Met Office who generated and update the unique Central England Temperature data sequence.

References

[1] Lockwood M, Harrison R G, Woollings T and Solanki S K 2010 Are cold winters in Europe associated with low solar activity? *Environ. Res. Lett.* **5** 024001
[2] Lockwood M 2010 Solar change and climate: an update in the light of the current exceptional solar minimum *Proc. R. Soc.* A **466** 303–29
[3] Abreu J A *et al* 2008 For how long will the current grand maximum of solar activity persist? *Geophys. Res. Lett.* **35** L20109
[4] Lockwood M, Rouillard A P and Finch I D 2009 The rise and fall of open solar flux during the current grand solar maximum *Astrophys. J.* **700** 937–44
[5] Manley G 1974 Central England temperatures: monthly means 1659–1973 *Q. J. R. Meteorol. Soc.* **100** 389–405
[6] Parker D E, Legg T P and Folland C K 1992 A new daily central England temperature series, 1772–1991 *Int. J. Clim.* **12** 317–42
[7] Karoly D J and Stott P A 2006 Anthropogenic warming of central England temperature *Atmos. Sci. Lett.* **7** 81–5
[8] Hansard 2010 HC (House of Commons) Written Ministerial Statements for 21 December 2010 (available at http://www.parliament.the-stationery-office.com/pa/cm/cmtoday/cmwms/archive/101221.htm)
[9] Shindell D T, Schmidt G A, Miller R L and Rind D 2001 Northern hemisphere winter climate response to greenhouse gas, ozone, solar, and volcanic forcing *J. Geophys. Res.* **106** 7193–210
[10] Shindell D T, Schmidt G A, Mann M E, Rind D and Waple A 2001 Solar forcing of regional climate change during the maunder minimum *Science* **294** 2149–52

[11] Shindell D T, Schmidt G A, Miller R L and Mann M E 2003 Volcanic and solar forcing of climate change during the preindustrial era *J. Clim.* **16** 4094–107

[12] North G R and Stevens M J 1998 Detecting climate signals in the surface temperature record *J. Clim.* **11** 563–77

[13] Lean J L and Rind D H 2008 How natural and anthropogenic influences alter global and regional surface temperatures: 1889–2006 *Geophys. Res. Lett.* **35** L18701

[14] Kossobokov V, Le Mouël J-L and Courtillot V 2010 A statistically significant signature of multidecadal solar activity changes in atmospheric temperatures at three European stations *J. Atmos. Sol.-Terr. Phys.* **72** 595–606

[15] Le Mouël J-L, Courtillot V, Blanter E and Shnirman M 2008 Evidence for a solar signature in 20th-century temperature data from the USA and Europe *C. R. Geosci.* **340** 421–30

[16] Le Mouël J-L, Blanter E, Shnirman M and Courtillot V 2009 Evidence for solar forcing in variability of temperature and pressure in Europe *J. Atmos. Sol.-Terr. Phys.* **71** 1309–21

[17] Le Mouël J-L, Kossobokov V and Courtillot V 2010 A solar pattern in the longest temperature series from three stations in Europe *J. Atmos. Sol.-Terr. Phys.* **72** 62–76

[18] Yiou P, Bard E, Dandin P, Legras B, Naveau P, Rust H W, Terray L and Vrac M 2010 Statistical issues about solar-climate relations *Clim. Past Discuss.* **6** 461–87

[19] Legras B, Mestre O, Bard E and Yiou P 2010 On misleading solar-climate relationship *Clim. Past Discuss.* **6** 767–800

[20] Hegerl G, Luterbacher J, González-Rouco F, Tett S F B, Crowley T and Xoplaki E 2011 Influence of human and natural forcing on European seasonal temperatures *Nat. Geosci.* **4** 99–103

[21] Mann M E, Zhang Z, Rutherford S, Bradley R, Hughes M K, Shindell D, Ammann C, Faluvegi G and Ni F 2009 Global signatures of the little ice age and Medieval climate anomaly and plausible dynamical origins *Science* **326** 1256–60

[22] Trouet V, Esper J, Graham N E, Baker A, Scourse J D and Frank D C 2009 Persistent positive North Atlantic Oscillation mode dominated the Medieval climate anomaly *Science* **324** 78–80

[23] Luterbacher J *et al* 2001 The late Maunder minimum (1675–1715)—a key period for studying decadal scale climatic change in Europe *Clim. Change* **49** 441–62

[24] Wanner H, Pfister C, Brázdil R, Frich P, Frydendahl K, Jónsson T, Kington J, Lamb H H, Rosenørn S and Wishman E 1995 Wintertime European circulation patterns during the late Maunder minimum cooling period (1675–1704) *Theor. Appl. Clim.* **51** 167–75

[25] Barriopedro D, Garcia-Herrera R and Huth R 2008 Solar modulation of Northern Hemisphere winter blocking *J. Geophys. Res.* **113** D14118

[26] Woollings T, Lockwood M, Masato G, Bell C and Gray L 2010 Enhanced signature of solar variability in Eurasian winter climate *Geophys. Res. Lett.* **37** L20805

[27] Huth R, Pokorná L, Bochníček J and Hejda P 2006 Solar cycle effects on modes of low-frequency circulation variability *J. Geophys. Res.* **111** D22107

[28] Huth R, Kyselý J, Bochníček J and Hejda P 2008 Solar activity affects the occurrence of synoptic types over Europe *Ann. Geophys.* **26** 1999–2004

[29] Scaife A A, Knight J R, Vallis G K and Folland C K 2005 A stratospheric influence on the winter NAO and North Atlantic surface climate *Geophys. Res. Lett.* **32** L18715

[30] Woollings T, Charlton-Perez A, Ineson S, Marshall A G and Masato G 2010 Associations between stratospheric variability and tropospheric blocking *J. Geophys. Res.* **115** D06108

[31] Martius O, Polvani L M and Davies H C 2009 Blocking precursors to stratospheric sudden warming events *Geophys. Res. Lett.* **36** L14806

[32] Rind D, Shindell D, Perlwitz J, Lerner J, Lonergan P, Lean J and McLinden C 2004 The relative importance of solar and anthropogenic forcing of climate change between the Maunder minimum and the present *J. Clim.* **17** 906–29

[33] Lockwood M, Bell C, Woollings T, Harrison R G, Gray L J and Haigh J D 2010 Top-down solar modulation of climate: evidence for centennial-scale change *Environ. Res. Lett.* **5** 034008

[34] Haigh J D 1996 The impact of solar variability on climate *Science* **272** 981–4

[35] Gray L J, Crooks S, Pascoe C, Sparrow S and Palmer M 2004 Solar and QBO influences on the timing of stratospheric sudden warmings *J. Atmos. Sci.* **61** 2777–96

[36] Simpson I R, Blackburn M and Haigh J D 2009 The role of eddies in driving the tropospheric response to stratospheric heating perturbations *J. Atmos. Sci.* **66** 1347–65

[37] Lockwood M, Stamper R and Wild M N 1999 A doubling of the sun's coronal magnetic field during the last 100 years *Nature* **399** 437–9

[38] Lockwood M and Owens M J 2011 Centennial changes in the heliospheric magnetic field and open solar flux: The consensus view from geomagnetic data and cosmogenic isotopes and its implications *J. Geophys. Res.* **116** A04109

[39] Vieira L E A and Solanki S K 2010 Evolution of the solar magnetic flux on time scales of years to millennia *Astron. Astrophys.* **509** A100

[40] Steinhilber F, Beer J and Fröhlich C 2009 Total solar irradiance during the Holocene *Geophys. Res. Lett.* **36** L19704

[41] Krivova N A, Balmaceda L and Solanki S K 2007 Reconstruction of solar total irradiance since 1700 from the surface magnetic flux *Astron. Astrophys.* **467** 335–46

[42] Robock A 2000 Volcanic eruptions and climate *Rev. Geophys.* **38** 191–219

[43] Robock A 2002 Pinatubo eruption—the climatic aftermath *Science* **295** 1242–4

[44] Jones G S, Gregory J M, Stott P A, Tett S F B and Thorpe R B 2005 An AOGCM simulation of the climate response to a volcanic super-eruption *Clim. Dyn.* **25** 725–38

[45] Fischer E M, Luterbacher J, Zorita E, Tett S F B, Casty C and Wanner H 2007 European climate response to tropical volcanic eruptions over the last half millennium *Geophys. Res. Lett.* **34** L05707

[46] Gao C, Robock A and Ammann C 2008 Volcanic forcing of climate over the past 1500 years: an improved ice-core-based index for climate models. *J. Geophys. Res.* **113** D23111

[47] de Jager C 2008 Solar activity and its influence on climate *Neth. J. Geosci.—Geol. En Mijnb.* **87** 207–13

[48] Beer J 2000 Neutron monitor records in broader historical context *Space Sci. Rev.* **93** 107–19

[49] Solanki S K, Usoskin I G, Kromer B, Schüssler M and Beer J 2004 Unusual activity of the Sun during recent decades compared to the previous 11 000 years *Nature* **431** 1084–7

[50] Vonmoos M, Beer J and Muscheler R 2006 Large variations in Holocene solar activity: constraints from ^{10}Be in the Greenland Ice Core Project ice core *J. Geophys. Res.* **111** A10105

[51] Muscheler R, Joos F, Beer J, Müller S A, Vonmoos M and Snowball I 2007 Solar activity during the last 1000 yr inferred from radionuclide records *Quat. Sci. Rev.* **26** 82–97

[52] McCracken K G 2004 Geomagnetic and atmospheric effects upon the cosmogenic ^{10}Be observed in polar ice *J. Geophys. Res.* **109** A04101

[53] Steinhilber F, Abreu J A and Beer J 2008 Solar modulation during the Holocene *Astrophys. Space Sci. Trans.* **4** 1–6

[54] Masarik J and Beer J 1999 Simulation of particle fluxes and cosmogenic nuclide production in the Earth's atmosphere *J. Geophys. Res.* **104** 12099–111

[55] Caballero-Lopez R A and Moraal H 2004 Limitations of the force field equation to describe cosmic ray modulation *J. Geophys. Res.* **109** A01101
[56] Steinhilber F, Abreu J A, Beer J and McCracken K G 2010 Interplanetary magnetic field during the past 9300 years inferred from cosmogenic radionuclides *J. Geophys. Res.* **115** A01104
[57] Lockwood M and Fröhlich C 2007 Recent oppositely directed trends in solar climate forcings and the global mean surface air temperature *Proc. R. Soc.* A **463** 2447–60
[58] Cattiaux J, Vautard R, Cassou C, Yiou P, Masson-Delmotte V and Codron F 2010 Winter 2010 in Europe: a cold extreme in a warming climate *Geophys. Res. Lett.* **37** L20704
[59] Woollings T 2010 Dynamical influences on European climate: an uncertain future *Phil. Trans.* A **368** 3733–56
[60] Meehl G A *et al* 2007 Global climate projections *Climate Change 2007: The Physical Science Basis. Contribution of Working Group I to the Fourth Assessment Report of the Intergovernmental Panel on Climate Change* ed S Solomon, D Qin, M Manning, Z Chen, M Marquis, K B Averyt, M Tignor and H L Miller (Cambridge: Cambridge University Press)
[61] Seierstad I A and Bader J 2009 Impact of a projected future Arctic Sea ice reduction on extratropical storminess and the NAO *Clim. Dyn.* **33** 937–43
[62] Petoukhov V and Semenov V A 2010 A link between reduced Barents-Kara sea ice and cold winter extremes over northern continents *J. Geophys. Res.* **115** D21111
[63] Hübener H, Cubasch U, Langematz U, Spangehl T, Niehörster F, Fast I and Kunze M 2007 Ensemble climate simulations using a fully coupled ocean–troposphere–stratosphere general circulation model *Phil. Trans. R. Soc.* A **365** 2089–101
[64] Selten F M, Branstator G, Kliphuis M and Dijkstra H A 2004 Tropical origins for recent and future Northern Hemisphere climate change *Geophys. Res. Lett.* **31** L21205
[65] Joshi M M, Charlton A J and Scaife A A 2006 On the influence of stratospheric water vapour changes on the tropospheric circulation *Geophys. Res. Lett.* **33** L09806
[66] Písek J and Brázdil R 2006 Responses of large volcanic eruptions in the instrumental and documentary climatic data over central Europe *Int. J. Climatol.* **26** 439–59
[67] Pozo-Vázquez D, Esteban-Parra M J, Rodrigo F S and Castro-Díez Y 2001 The association between ENSO and Winter Atmospheric Circulation and Temperature in the North Atlantic Region *J. Clim.* **14** 3408–20
[68] Ineson S and Scaife A A 2009 The role of the stratosphere in the European climate response to El Niño *Nat. Geosci.* **2** 32–6
[69] Franzke C and Woollings T 2011 On the persistence and predictability properties of North Atlantic climate variability *J. Clim.* **24** 466–72
[70] Street R B, Steynor A, Bowyer P and Humphrey K 2009 Delivering and using the UK climate projections 2009 *Weather* **64** 227–31
[71] Jung T, Vitart F, Ferranti L and Morcrette J-J 2011 Origin and predictability of the extreme negative NAO winter of 2009/10 *Geophys. Res. Lett.* **38** L07701
[72] Lockwood M 2011 Was spectral solar irradiance lower during the recent low sunspot minimum? *J. Geophys. Res.* at press (doi:10.1029/2010JD014746)